Third International Conference on Multiphase Flow, ICMF'98
Lyon, France, June 8–12, 1998.
CD–ROM Proceedings, Paper No. 217

LAGRANGIAN PREDICTION OF DISPERSE GAS–PARTICLE FLOW IN CYCLONE SEPARATORS

Th. Frank, E. Wassen, Q. Yu
Technical University of Chemnitz
Faculty of Mechanical Engineering and Process Technology
Research Group of Multiphase Flow
Chemnitz, Germany

1 Introduction

Disperse multiphase flows are very common for processes in mechanical and thermal process technology (e.g. gas–particle or gas–droplet flows, coal combustion, pneumatical conveying, erosion phenomena). Processes for the separation of solid particles from gases or fluids and for the classification and particle size analysis are an important field of interest in process technology. Most flow regimes in technical processes are real 3–dimensional and cannot be restricted to 2–dimensional numerical analysis. Therefore the paper deals with a Lagrangian approach for the prediction of 3–dimensional, disperse gas–particle flows and its application for flow simulation in cyclone particle separators.

The investigations of the precipitation of quartz particles were carried out for a series of four geometrically similiar cyclones of different size and for a number of different gas inlet velocities. Numerical results were compared with experiments by König [3] and show a very good agreement with experimentally predicted particle precipitation rates.

2 Basic Equations of Fluid Motion

The 3–dimensional, two–phase (gas–particle) flow in the cyclone separator is described by assuming that the particulate phase is dilute and that the particle loading is rather low. This assumption satisfies the neglect of inter–particle effects and contributing source terms in the Navier–Stokes equations due to particle–fluid interaction. Further the two–phase flow is assumed statistically steady, incompressible and isothermal. Then the time–averaged form of the governing gas phase equations can be expressed in the form of the general transport equation :

$$\begin{aligned} \frac{\partial}{\partial x}(\rho_F\, u_F\, \Phi) \;+\; \frac{\partial}{\partial y}(\rho_F\, v_F \Phi) \;+\; \frac{\partial}{\partial z}(\rho_F\, w_F \Phi) \;=\; \\ \frac{\partial}{\partial x}\left(\Gamma_\Phi \frac{\partial \Phi}{\partial x}\right) + \frac{\partial}{\partial y}\left(\Gamma_\Phi \frac{\partial \Phi}{\partial y}\right) + \frac{\partial}{\partial z}\left(\Gamma_\Phi \frac{\partial \Phi}{\partial z}\right) + S_\Phi + S_\Phi^P \end{aligned} \tag{1}$$

Here Φ is a general variable, Γ_Φ a diffusion coefficient, S_Φ a general source term and S_Φ^P is the source term due to particle–fluid interaction ($S_\Phi^P \equiv 0$ if coupling of the continous and disperse phase can be neglected). The relationship of S_Φ, Γ_Φ, S_Φ and S_Φ^P and the constants of the standard k–ε turbulence model used for the present numerical simulation are given in Table 1.

3 Equations of Motion of the Disperse Phase

The disperse phase is treated by the application of the Lagrangian approach, i.e. discrete particle trajectories are calculated. Each calculated particle represents a large number of physical particles of the same physical properties which is characterized by the particle flow rate $\dot{N}_P$ along each calculated particle trajectory. The prediction of the particle trajectories is carried out by solving the ordinary differential equations for the particle location and velocities. Assuming that the ratio of fluid to particle density is

Φ	S_Φ	S_Φ^P	Γ
1	0	0	0
u_F	$\frac{\partial}{\partial x}\left(\Gamma_\Phi \frac{\partial u_F}{\partial x}\right) + \frac{\partial}{\partial y}\left(\Gamma_\Phi \frac{\partial v_F}{\partial x}\right) + \frac{\partial}{\partial z}\left(\Gamma_\Phi \frac{\partial w_F}{\partial x}\right) - \frac{\partial p}{\partial x} + \rho_F f_x$	$S_{u_F}^P$	μ_{eff}
v_F	$\frac{\partial}{\partial x}\left(\Gamma_\Phi \frac{\partial u_F}{\partial y}\right) + \frac{\partial}{\partial y}\left(\Gamma_\Phi \frac{\partial v_F}{\partial y}\right) + \frac{\partial}{\partial z}\left(\Gamma_\Phi \frac{\partial w_F}{\partial y}\right) - \frac{\partial p}{\partial y} + \rho_F f_y$	$S_{v_F}^P$	μ_{eff}
w_F	$\frac{\partial}{\partial x}\left(\Gamma_\Phi \frac{\partial u_F}{\partial z}\right) + \frac{\partial}{\partial y}\left(\Gamma_\Phi \frac{\partial v_F}{\partial z}\right) + \frac{\partial}{\partial z}\left(\Gamma_\Phi \frac{\partial w_F}{\partial z}\right) - \frac{\partial p}{\partial z} + \rho_F f_z$	$S_{w_F}^P$	μ_{eff}
k	$P_k - \rho_F\,\varepsilon$	0	$\frac{\mu_t}{\sigma_k}$
ε	$\frac{\varepsilon}{k}(c_{\varepsilon_1} P_k - c_{\varepsilon_2}\,\rho_F\,\varepsilon)$	0	$\frac{\mu_t}{\sigma_\varepsilon}$
$P_k = \mu_t \left\{ 2 \cdot \left[\left(\frac{\partial u_F}{\partial x}\right)^2 + \left(\frac{\partial v_F}{\partial y}\right)^2 + \left(\frac{\partial w_F}{\partial z}\right)^2 \right] + \left(\frac{\partial u_F}{\partial y} + \frac{\partial v_F}{\partial x}\right)^2 + \left(\frac{\partial u_F}{\partial z} + \frac{\partial w_F}{\partial x}\right)^2 + \left(\frac{\partial w_F}{\partial y} + \frac{\partial v_F}{\partial z}\right)^2 \right\}$			
$\mu_{eff} = \mu + \mu_t \quad , \quad \mu_t = \rho_F c_\mu \frac{k^2}{\varepsilon}$ $c_\mu = 0.09 \quad , \quad c_{\varepsilon_1} = 1.44 \quad , \quad c_{\varepsilon_2} = 1.92 \quad , \quad \sigma_k = 1.0 \quad , \quad \sigma_\varepsilon = 1.3$			

Table 1: Source terms and transport coefficients for different variables Φ

small ($\rho_F/\rho_P \ll 1$) these equations read :

$$\frac{d}{dt}\begin{bmatrix} x_P \\ y_P \\ z_P \end{bmatrix} = \begin{bmatrix} u_P \\ v_P \\ w_P \end{bmatrix} \tag{2}$$

$$\begin{aligned} \frac{d}{dt}\begin{bmatrix} u_P \\ v_P \\ w_P \end{bmatrix} &= \frac{3}{4}\frac{\rho_F}{(\rho_P + \frac{1}{2}\rho_F) d_P} \left(v_{rel} C_D(Re_P) \begin{bmatrix} u_F - u_P \\ v_F - v_P \\ w_F - w_P \end{bmatrix} \right. \\ &+ \left. \frac{2\nu_F^{1/2}}{\pi |\vec{\Omega}|^{1/2}} C_A \begin{bmatrix} (v_F - v_P)\Omega_z - (w_F - w_P)\Omega_y \\ (w_F - w_P)\Omega_x - (u_F - u_P)\Omega_z \\ (u_F - u_P)\Omega_y - (v_F - v_P)\Omega_x \end{bmatrix} \right) + \frac{\rho_P - \rho_F}{\rho_P + \frac{1}{2}\rho_F} \begin{bmatrix} g_x \\ g_y \\ g_z \end{bmatrix} \end{aligned} \tag{3}$$

with

$$\vec{\Omega} = \text{rot}\ \vec{v}_F \quad , \quad Re_P = \frac{d_P\, v_{rel}}{\nu_F} \quad , \quad v_{rel} = \sqrt{(u_F - u_P)^2 + (v_F - v_P)^2 + (w_F - w_P)^2}$$

These equations of motion of the disperse phase include at the right hand side the drag force, the lift force due to shear in the fluid flow field (Saffman force), the gravitational and added mass force. For the present numerical investigation the Magnus force due to particle rotation is neglected because of there minor importance for the very fine particles in the particle diameter range of interest.

The values for the coefficients C_D and C_A can be found in literature [1, 9]. Additionally for the lift coefficient C_A the correction obtained by Mei [4, 9] is taken into account. The effect of fluid turbulence on the motion of the disperse phase, which is regarded to be very important for the particle diameter range under investigation, is modelled by the Lagrangian Stochastic–Deterministic (LSD) turbulence model proposed by Schönung and Milojević [5]. The particle–wall collisions are treated according to the irregular bouncing model by Sommerfeld [8, 9] in the modified wall roughness formulation given in [10, 1].

4 Solution Algorithm

The time–averaged equations of fluid motion are solved using the program package FAN–3D developed by Perić and Lilek [6, 7]. The program FAN–3D was extensively modified by the authors for gas–particle

flow computations. Further modifications involve the implementation of a standard k–ε turbulence model and the parallelization of the solution algorithm by application of a domain decomposition method. The most fundamental features of FAN–3D are :

- use of non–orthogonal, boundary fitted, numerical grids with arbitrary hexahedral control volumes,
- use of block structured numerical grids for geometrical approximation of complex flow domains;
- parallelization using domain decomposition method;
- finite volume solution approach of SIMPLE kind with colocated variable arrangement; Cartesian vector and tensor components;

The solution algorithm for the equations of particle motion is based on the program package PartFlow developed by the authors. A detailed description of the 3–dimensional solution algorithm and the developed parallelization methods for the Lagrangian approache can be found in [1, 2].

5 Gas–Particle Flow in a Standard Cyclone

The presented 3–dimensional Lagrangian approach was applied to the gas–particle flow in a standard cyclone (Fig. 1). The calculations were based on experimental investigations carried out by König [3] on a series of geometrically similiar cyclones for a number of different inlet gas velocities.

5.1 Flow Geometry and the Numerical Grid

The cyclones Z10, Z20, Z40 and Z80 investigated in this paper were determined by the following geometrical properties (see also Fig. 1) :

		Z10	Z20	Z40	Z80
Diameter of the cyclon	D	40 mm	80 mm	160 mm	320 mm
Height of the cyclon	H	195 mm	390 mm	780 mm	1560 mm
Inlet cross section	$a \times b$	4.5×18 mm^2	9×36 mm^2	18×72 mm^2	36×144 mm^2
Diameter of the gas exit	d_T	10 mm	20 mm	40 mm	80 mm
Height of the gas exit	h_T	31 mm	62 mm	124 mm	248 mm
Diameter of the particle exit	d_B	10 mm	20 mm	40 mm	80 mm

Due to the complex geometry of the cyclone a numerical grid with 42 different grid blocks and about 250.000 finite volume elements had to be designed for the numerical calculations of the gas–particle flow (Fig. 2). The numerical grid was originally designed for the Z10 cyclone and then proportionally scaled as $1:2:4:8$ for the other three cyclones Z20–Z80.

5.2 Prediction of the Gas and Particle Flow, Pressure Loss

In the course of first calculations of the gas flow field in the cyclones it was found that the numerical mesh needed further improvement and certain grid refinement in regions of large fluid velocity gradients in order to get converged solutions. Grid refinement was applied to the gas inlet and to the region in the vicinity of the lower end of the gas exit tube. But certain restrictions in the mesh generation algorithm prevented an optimum arrangement and design of the finite volume elements in some regions of the flow geometry. Consequently strong underrelaxation had to be applied for the solution algorithm in order to obtain convergence, mainly due to the convergence behavior of the k–ε equations.

Unfortunately there is no data material about the velocity fields in the Z10,...,Z80 cyclones in the publication of König. But the flow in cyclone separators was studied in the past by many authors and thus the calculated flow field can be assessed at least qualitatively. Fig. 3 shows the mean gas velocity distribution in the upper part of the cyclone. Calculated flow fields show the typical asymetrical main vortex in the upper cylindrical part of the cyclone. In a more detailed view [11] a flow recirculation can be found along the lid of this cylindrical part of the cyclone and further downwards along the outer wall of the gas exit tube. This kind of recirculating flow is well known for cyclone separators from literature. The flow field in the other parts of the cyclone is also in qualitative agreement with the knowledge available for the flow in cyclone separators.

For further comparison the pressure loss over the cyclone was predicted for various gas inlet velocities and compared with the experimental data of König (Fig. 5). The pressure loss data of König take only into account the difference of the static pressure before and after the cyclone. The diagram shows an underprediction of the pressure loss obtained from the numerical calculations for all investigated gas inlet

velocities. The reason for that is most likely to be found in slight differences between the experimental setup and the flow geometry investigated numerically. The numerical data of the pressure loss show a comparable increase with increasing gas inlet velocity.

Particle trajectory calculations were carried out using the described Lagrangian approach with the predicted gas flow fields in order to obtain particle precipitation rates for the four different cyclones (see Fig. 5). Main difficulties in the calculation of particle motion could be observed in the following :

1. The flow in the cyclone leeds to a very large number of particle–wall collisions. The detection of a particle–wall collision results in a decrease of the integration time step of the solution algorithm. Therefore the large number of particle–wall collisions leed to large computation time for the prediction of the particle motion.
2. The large computation time needed for cyclone flow prediction is also determined by consideration of the influence of gas flow turbulence on particle motion. In order to ensure accuracy the integration time step is set to be less then 1/10 of the turbulent time scale of the LSD turbulence model. The resulting small time steps of the Runge–Kutta solver for the particle equations of motion contribute to the large computational effort needed for the present simulation.
3. The larger geometrical size of the Z40 and Z80 cyclones leed to a substantial increase of particle residence time in the cyclone and thus to larger computation time.

As a result the calculation of about 10.000 particle trajectories in the cyclon separator takes about 22 hours of CPU–time on a single MIPS R10000 processor of a Silicon Graphics CRAY Origin2000.

5.3 Calculation of the Particle Precipitation Rate

In accordance with the experiments of König [3] the investigations for the prediction of the particle precipitation rate were carried out for the physical properties of a fraction of quartz particles of the Busch company. The original quartz dust had a particle diameter distribution in the range of $d_P = 0 \ldots 50\ \mu m$ with a mean particle diameter of $\overline{d_P} = 10.9\ \mu m$. The numerical simulations were carried out for 20 particle diameter classes in the range between $0.5 \ldots 15\ \mu m$. A total number of 670 particle trajectories with random initial conditions in the inlet cross section were calculated for each of the 20 particle diameter classes. Even not stated in the publication of König a particle density of $\rho_P = 2500\ kg/m^3$ was assumed for the quartz particles. For the coefficients of restitution and kinetic friction typical values for quartz particles were used ($k = 0.8$, $f = 0.35$).

In a first series of calculations the precipitation rates for the quartz particles were predicted for all four cyclones Z10,. . .,Z80 with an inlet gas velocity of $u_F = 10\ m/s$. Then the precipitation rate can be predicted as :

$$T(d_P) = 1 - \frac{\dot{N}_{out}(d_P)}{\dot{N}_{in}(d_P)}$$

where $\dot{N}_{in}(d_P)$ and $\dot{N}_{out}(d_P)$ are the particle flow rates for a given particle size in the inlet cross section and gas exit cross section respectively. In the numerical prediction particles are assumed to be precipitated in the cyclone, if :

1. The particle trajectory reaches the particle exit cross section.
2. The particle sticks to the wall of the cyclone (that means the wall normal velocity of the particle after a particle–wall collision is less than $10^{-5}\ m/s$).
3. The particle residence time in the cyclone is larger than the maximum allowed computation time, which was set to $T_{max} = 150\ s$ for Z10, Z20 and to $T_{max} = 250\ s$ for cyclones Z40, Z80 due to there larger geometrical size. The value for T_{max} was choosen in a way, that the number of particles with this very large residence time in the cyclone was less than 4–5 % of the calculated particle trajectories.

Fig. 6–9 show the comparison of the numerically predicted particle precipitation rates with the experimental results of König. The figures show for all four different cyclones a very good agreement of the numerical and experimental results. The shape of the precipitation rate curves is nearly identical, even if for the smaller cyclones Z10 and Z20 a slight shift of the precipitation rate curve towards higher particle diameters can be observed. For the Z40 and Z80 cyclones actually no difference between the numerical and experimental results can be found.

In a second step the gas inlet velocity for the Z20 cyclone was varied. Fig. 10 shows the results for the two gas inlet velocities $u_F = 4.3\ m/s$ and $u_F = 10\ m/s$. Again the experimentally and numerically predicted precipitation rates are in very good agreement. Furthermore the numerical simulation gives

the right tendency of a shift of the cut–off particle diameter towards larger particles for decreased gas inlet velocities. This result could also be established in numerical simulations for the other cyclones with varied gas inlet velocity.

6 Conclusions

The paper gives the formulation of a 3–dimensional Lagrangian approach applicable to flow domains with complex geometrical boundary conditions. The Lagrangian approach is applied to the gas–particle flow in a series of four geometrically similiar cyclones with different gas inlet velocities. The paper presents the numerical results for the predicted pressure loss and particle precipitation rates. The comparison with the results of König [3] show the very good agreement of the numerical results with experimental data.

7 Acknoledgement

The authors thank Prof. M. Perić for the provision of his CFD code FAN–3D for this research. Further this work was supported by the Deutsche Forschungsgemeinschaft (DFG) under Contract No. SFB 393/D2.

References

[1] Frank Th., Wassen E., Q. Yu, 1997, "A 3–dimensional Lagrangian Solver for Disperse Multiphase Flows on Arbitrary, Geometricaly Complex Flow Domains using Block–structured Numerical Grids", *7th Int. Symposium on Gas-Particle Flows*, ASME Fluids Engineering Division Summer Meeting, Vancouver, BC, Canada, June 22–26, 1997, CD–ROM Proceedings, FEDSM97–3590.

[2] Frank Th., Wassen E., 1997, "Parallel Efficiency of PVM– and MPI–Implementations of two Algorithms for the Lagrangian Prediction of Disperse Multiphase Flows", *JSME Centennial Grand Congress 1997*, ISAC '97 Conference on Advanced Computing on Multiphase Flow, Tokyo, Japan, July 18–19, 1997.

[3] König C., 1990, "Untersuchungen zum Abscheideverhalten von geometrisch ähnlichen Zyklonen", PhD Thesis, University of Kaiserslautern, Germany.

[4] Mei R., 1992, "An approximate expression for the shear lift force on a spherical particle at finite Reynolds number", *Int. J. Multiphase Flow*, Vol. 18, pp. 145–147.

[5] Milojević, D., 1990, "Lagrangian Stochastic–Deterministic (LSD) Predictions of Particle Dispersion in Turbulence", *Part. Part. Syst. Charact.*, Vol. 7, pp. 181–190.

[6] Perić M., 1992, "Ein zum Parallelrechnen geeignetes Finite–Volumen–Mehrgitterverfahren zur Berechnung komplexer Strömungen auf blockstrukturierten Gittern mit lokaler Verfeinerung", Abschlußbericht zum DFG–Vorhaben Pe 350/3–1 im DFG–Habilitandenstipendiumprogramm, Stanford University, USA.

[7] Schreck E., Perić M., 1992, "Parallelization of implicit solution methods", *ASME Fluids Engineering Conference*, June 22–23, 1992, Los Angeles (CA), USA.

[8] Sommerfeld M., 1992, "Modelling of particle–wall collisions in confined gas–particle flows", *Int. Journal of Multiphase Flows*, Vol. 18, No. 6, pp. 905–926.

[9] Sommerfeld M., 1996, "Modellierung und numerische Berechnung von partikelbeladenen turbulenten Strömungen mit Hilfe des Euler/Lagrange–Verfahrens", Berichte aus der Strömungstechnik, Shaker Verlag, Aachen, Germany.

[10] Tsuji Y., Shen N.Y., Morikawa Y., 1991, "Lagrangian Simulation of Dilute Gas–Solid Flows in a Horizontal Pipe", *Advanced Powder Technology*, Vol. 2, No. 1, pp. 63–81.

[11] Web site of the Research Group on Multiphase Flow, Technical University Chemnitz, Germany.
http://www.tu-chemnitz.de/mbv/FAK/TechnThDyn/mpf/e/index.html – Index.
http://www.tu-chemnitz.de/mbv/FAK/TechnThDyn/mpf/mpf_lit.html – List of Publications.

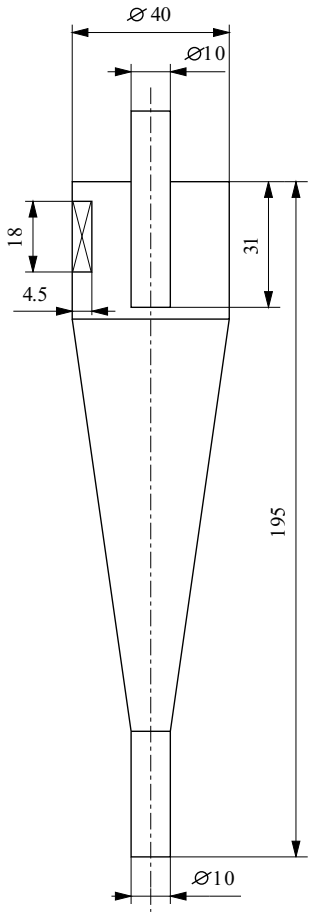

Figure 1: Scheme of the standard cyclone Z10.

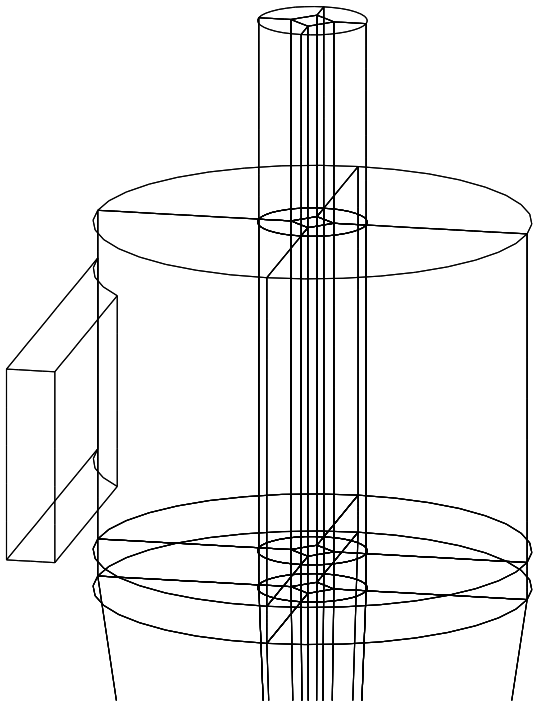

Figure 2: Block structure of the numerical grid in the upper part of the cyclone.

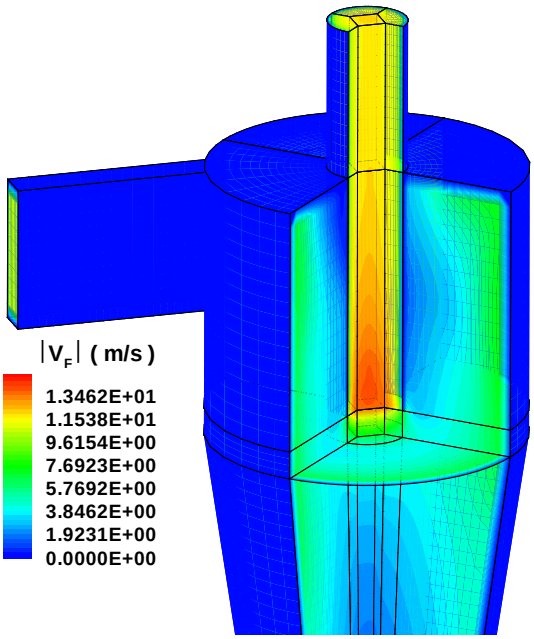

Figure 3: Mean gas velocity distribution in the upper part of Z10 near the gas exit, $u_F = 10\ m/s$.

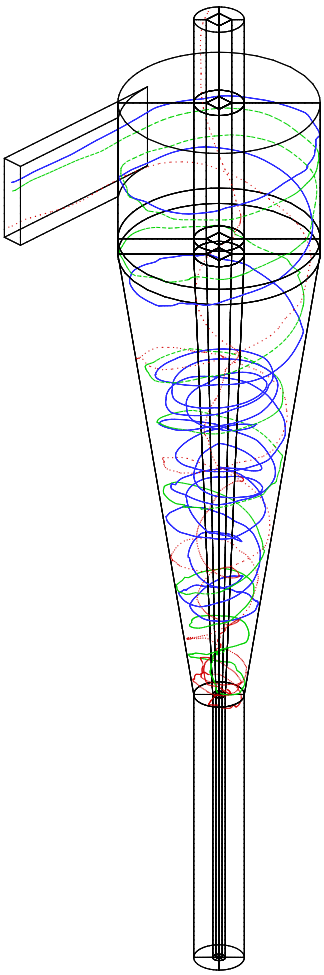

Figure 4: Particle trajectories in Z10 for gas inlet velocity $u_F = 10\ m/s$, $d_P = 1, \ldots, 5\ \mu m$.

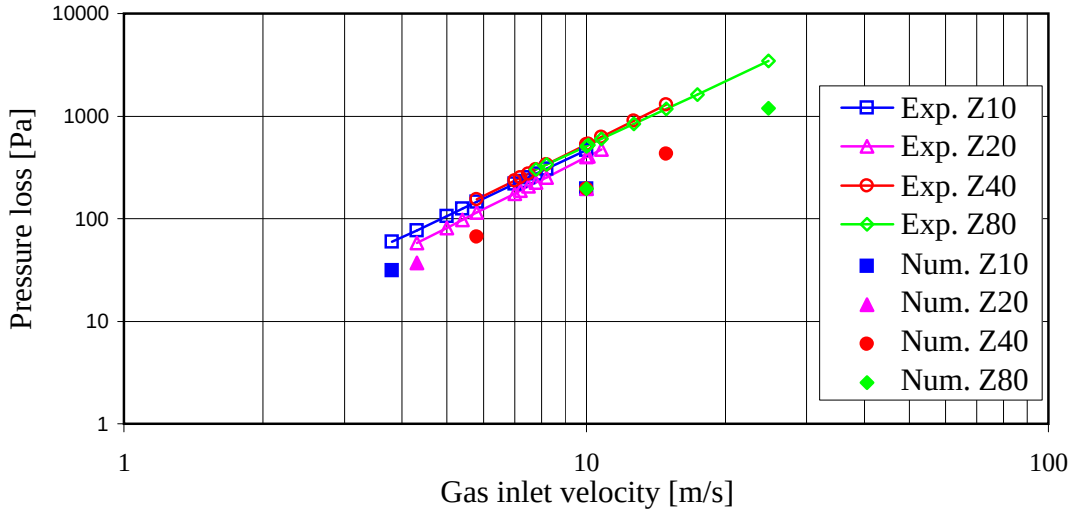

Figure 5: Comparison of pressure loss vs. gas inlet velocity for Z10,. . .,Z80 cyclones.

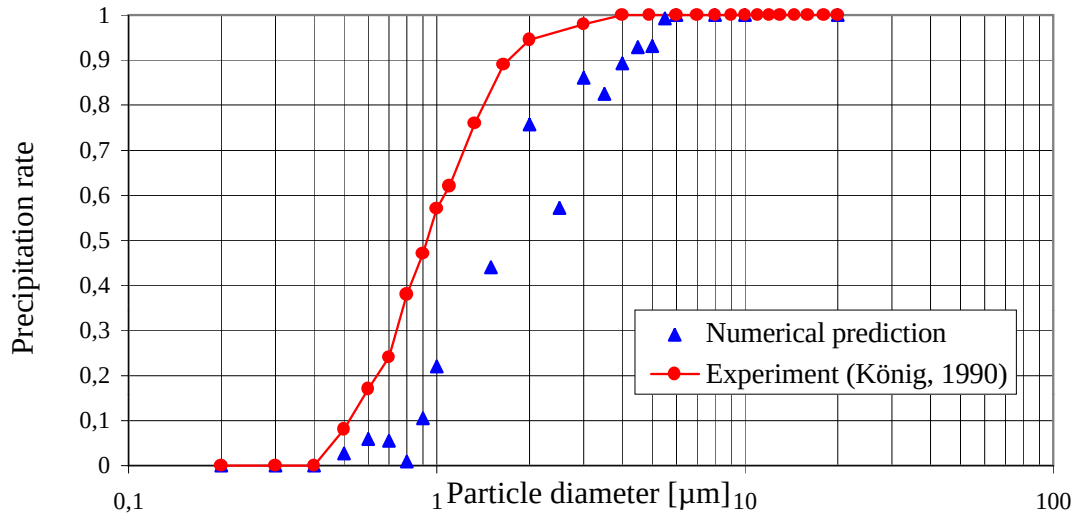

Figure 6: Comparison of the precipitation rate for the Z10 cyclone, $u_F = 10\ m/s$.

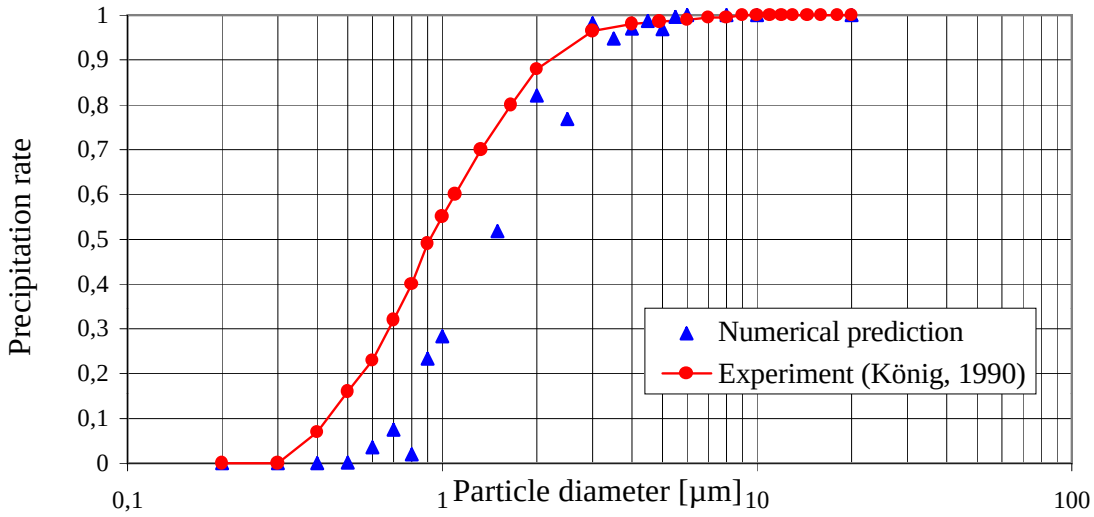

Figure 7: Comparison of the precipitation rate for the Z20 cyclone, $u_F = 10\ m/s$.

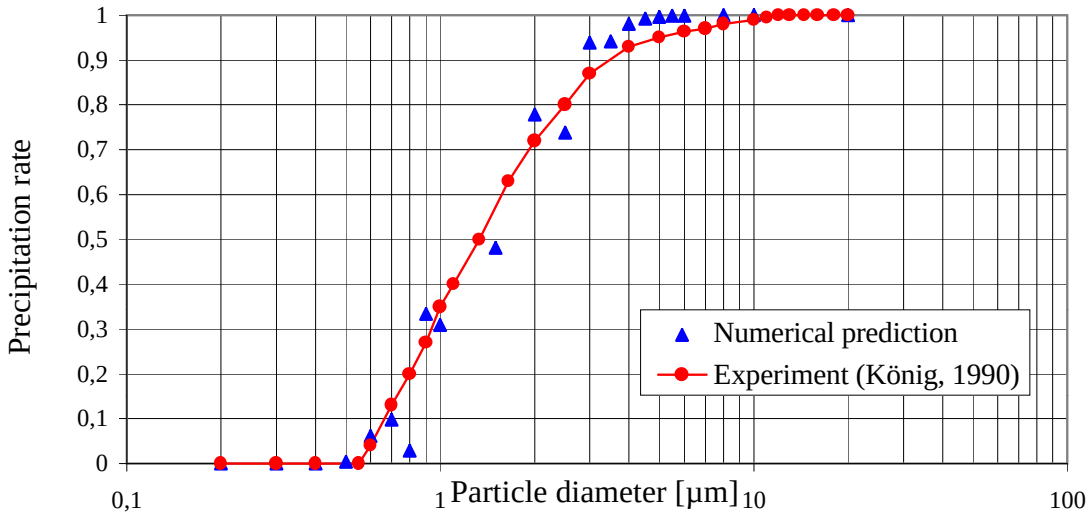

Figure 8: Comparison of the precipitation rate for the Z40 cyclone, $u_F = 10\ m/s$.

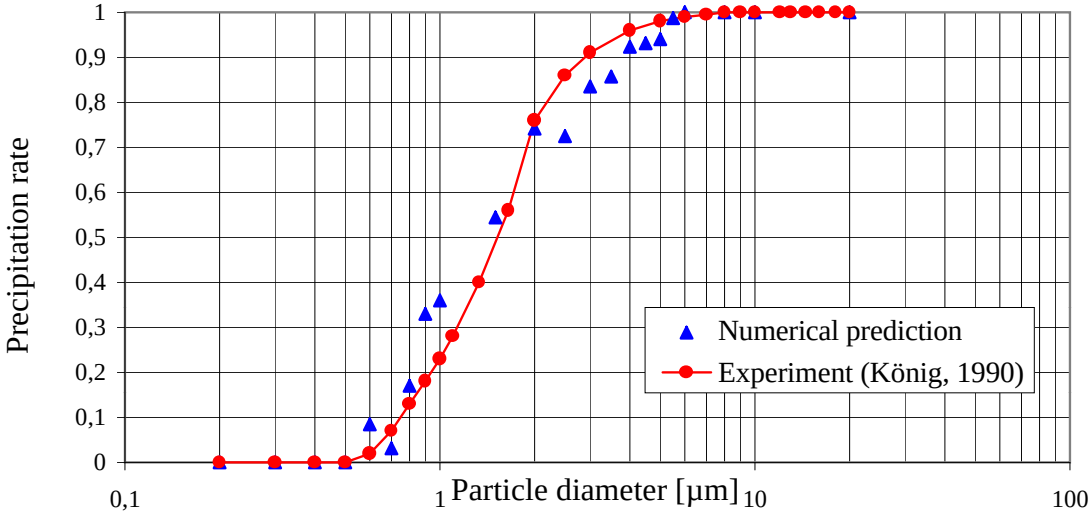

Figure 9: Comparison of the precipitation rate for the Z80 cyclone, $u_F = 10\ m/s$.

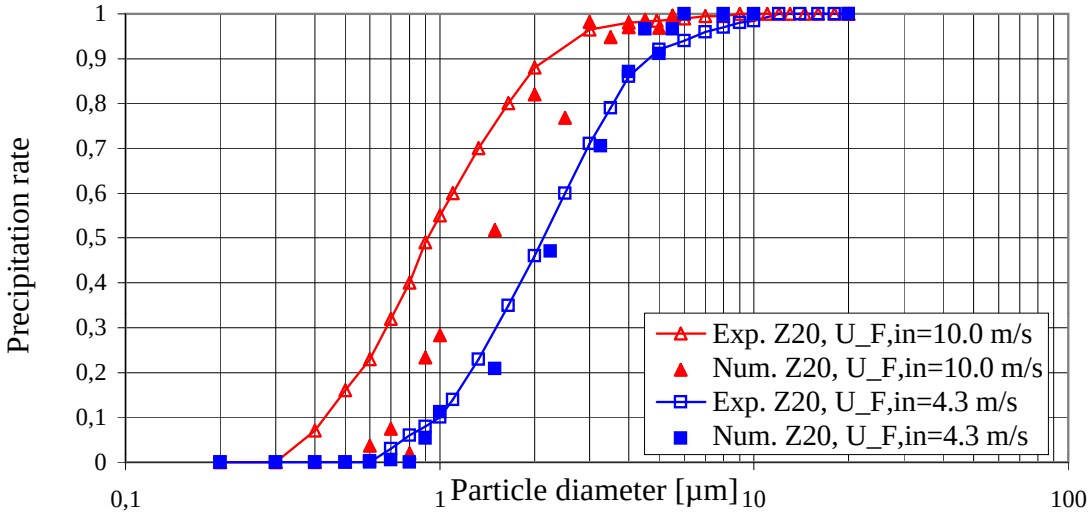

Figure 10: Comparison of precipitation rates for Z20 and gas inlet velocities $u_F = 4.3\ m/s$ and $10\ m/s$.